J. Fluid Mech. (1982), *vol.* 114, *pp.* 27–40
Printed in Great Britain

Instability of a planar liquid layer in an alternating magnetic field

By E. J. McHALE AND J. R. MELCHER

Massachusetts Institute of Technology, Department of Electrical Engineering and Computer Science, Cambridge, Mass. 02139 U.S.A.

(Received 14 January 1980 and in revised form 25 March 1981)

Liquid metal interfaces, stressed by a high-frequency, alternating magnetic field are commonly observed to undulate. Even a planar interface stressed from above by a uniform magnetic field takes on an appearance that is very different from what is observed if the same layer is heated from below with about the same thermal input as associated with the eddy currents. This behaviour affects internal mixing and the transport of heat and material from interfaces. In applications where the interface is used to form glass or other materials, the undulations can be disasterous. A goal of this paper is to identify the circumstances under which this motion can be avoided. A theoretical model is developed for fluid motions, coupled to a magnetic flux density (having magnitude B_0 and angular frequency ω) through a force density that is time averaged over one period of the alternating field. This theory, which does not include thermal effects, predicts a threshold for onset of instability determined by the ratio of layer thickness to skin depth and by the parameter $M = B_0^2/\mu\eta\omega$, where $\mu = 4\pi \times 10^{-7}$ and η is the viscosity. The instability has an internal nature in that it is predicted even when the liquid is bounded by rigid insulating materials. Threshold measurements are reported that agree with the predictions over more than an order-of-magnitude variation in frequency, including low frequencies, for which the finite depth of the liquid layer is important. However, observed growth times are far shorter than predicted. It is concluded that the observed motions are in fact thermally driven, but take on an appearance dictated by the hydromagnetics. A previously developed lumped parameter model, which includes thermally driven motion, does predict growth times on the order of those observed. In the lumped parameter model the critical field strength grossly affects the nonlinear saturation velocity. The critical M sets an upper limit on the extent to which a liquid metal can be levitated, depressed or transported magnetically at a given frequency without incurring interfacial undulations and an augmentation of mass and heat transfer.

1. Description of phenomenon

Magnetic fields are commonly used to levitate and melt metals and to shape liquid interfaces. In those applications, where free surfaces give some hint of the bulk fluid motions, spontaneous undulations of the interface are commonly observed (Fraser *et al.* 1971; Sunderlam 1973; Melcher & Hurwitz 1970). Under more controlled conditions, they are also observed in the study of hydromagnetic surface waves (Schaffer 1966, 1968).

An apparatus for studying the phenomenon, shown in figure 1, consists of a set of

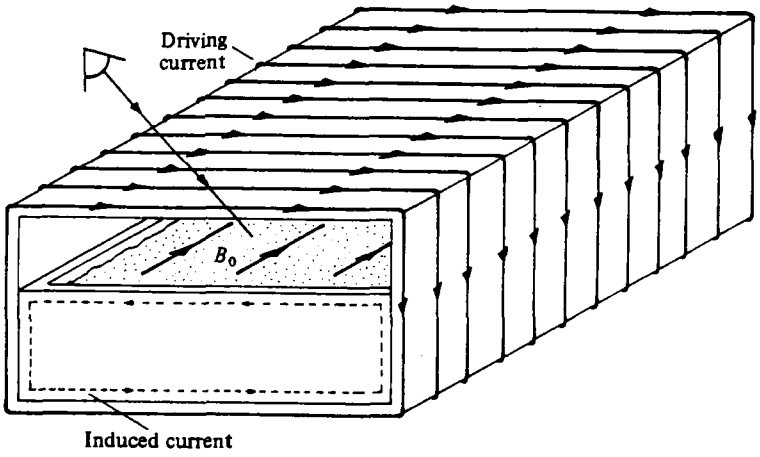

FIGURE 1. Experimental apparatus.

coils used to apply a nearly uniform audio frequency field to the surface of a dish of liquid metal. As the magnetic field is increased, a threshold is reached beyond which the fluid begins to undergo a distinctive unsteady corrugation. The interfacial motion, shown in the photographs of figure 2, consists of undulations having a frequency of approximately 0·5–2 Hz. When the field is turned on suddenly, the undulations appear and reach a saturation amplitude within 1–10 s. Edge effects associated with returning the currents that flow at the interface, can be sites of the convection. But, with care taken to minimize edge effects, there is apparently a well-defined change from a relatively quiescent state to one of random agitation as the field is raised. This motion differs in appearance from convection caused by heating the fluid unevenly or from below with an amount of heat that is essentially the same as that dissipated by the eddy currents. The surface undulations are also different in appearance from gravity–capillary surface waves. At typical observed wavelengths (1–10 cm) undulation frequencies are much less than those of a field-coupled gravity–capillary wave. Also, waves excited by striking the fluid contained have no similarity in appearance to the undulations.

Analysis shows (McHale 1977) that a non-uniform magnetic field can drive relatively large-scale cellular convection, leading at high fields to turbulence. When the corresponding experiment is performed, the appearance of the surface is typically much smoother than that described.

The model set forth in the following sections is aimed at identifying electromechanical contributions to these motions. In static equilibrium, the pressure equilibrates the magnetic force density, which is in the vertical direction. The model pictures the motions as resulting from an instability caused by a magnetic force density resulting from the motion of the fluid itself. In the development of this linear continuum theory, thermal effects associated with the joule heating from the eddy currents are ignored. In the discussion section, thermal effects are considered in the light of a nonlinear lumped-parameter model. In the linear stability theory, developed in §2, high-frequency components of the magnetic force are ignored. Fluid inertia and viscosity tend to prevent any appreciable motion at twice the frequency of the applied field (typically 2 kHz). This 'time-average force' model includes the self-consistent

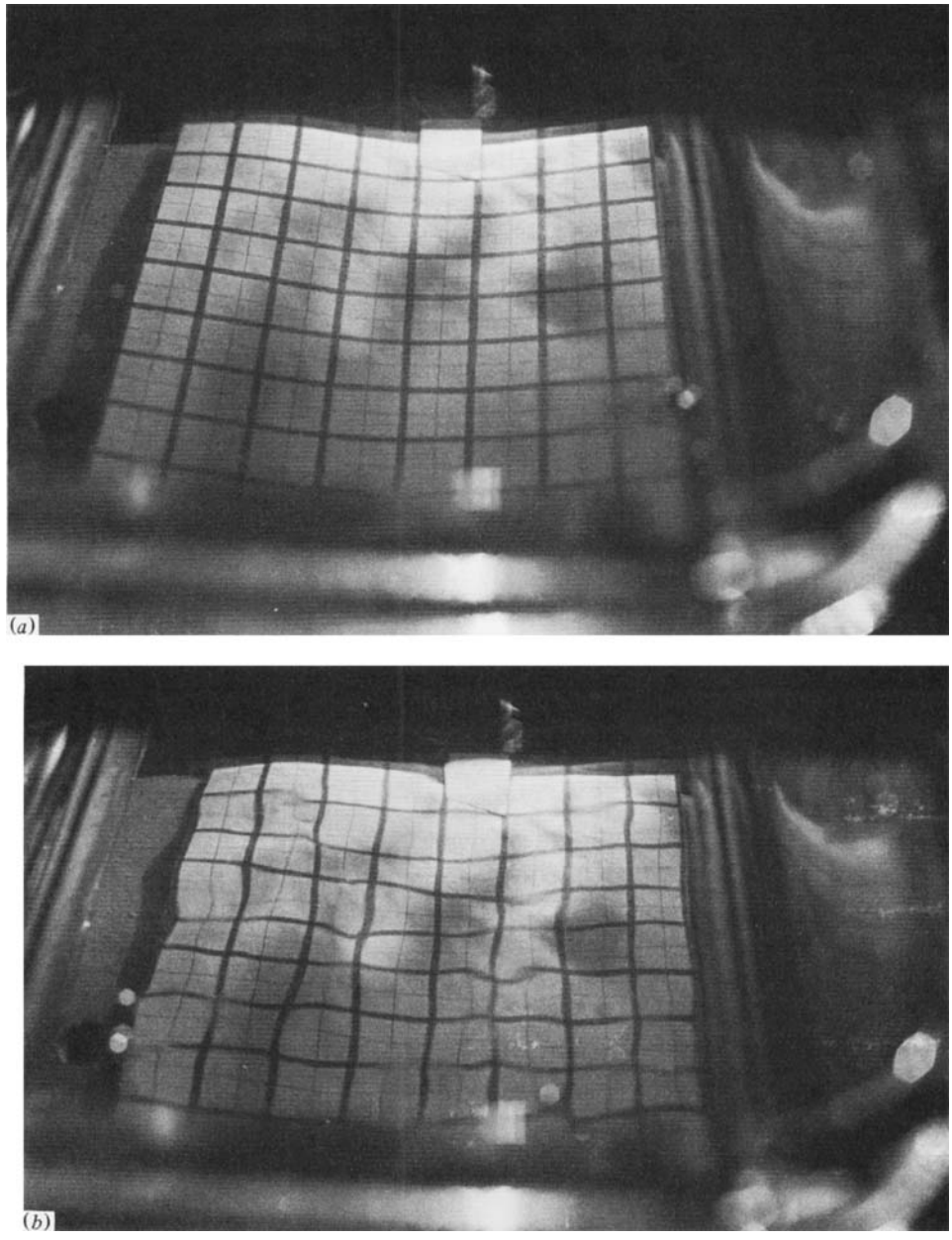

FIGURE 2. Photograph of surface reflecting grid lines for visualization of interface. Interface is viewed at angle through end of coil shown in figure 1. (*a*) Without field; (*b*) with a relatively intense field.

effects of the fluid motion on the field and results in a prediction of the critical field strength as well as the instability growth rate. Section 3 presents experimental results which are compared to the theory. Finally, §4 summarizes what can be concluded about the origins of the undulations based on the successes and inadequacies of the pure electromechanical model. A lumped-parameter model described elsewhere

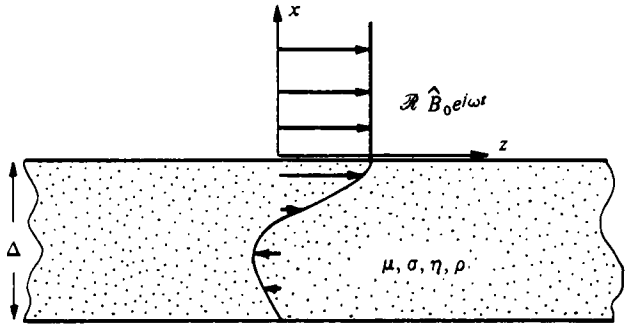

FIGURE 3. Schematic diagram of fluid layer shown in cross-section. Gravity acts in $-x$ direction.

includes thermal as well as electromechanical influences and helps to relate the electromechanics to the thermal-gravitational origins of the energy driving the instability.

2. Linear stability theory

It is possible that the interfacial motion is a non-essential consequence of internal instability. Thus, motions considered first are with the interface constrained. Then effects of surface deformation are taken up. First, the bulk relations that apply in either case are derived.

Bulk relations

For the equilibrium shown in figure 3, the fluid is at rest and the imposed z-directed magnetic field is uniform in the transverse y and z directions. The magnetic diffusion equation governs the space–time distribution in the liquid layer. For example, if the layer is thick compared to the skin depth $\delta \equiv (2/\omega\mu_0\sigma)^{\frac{1}{2}}$ then this equilibrium distribution is

$$\mathbf{B}_e = \mathscr{R}\, B_0\, e^{(1+j)x/\delta}\, e^{j\omega t}\, \mathbf{i}_z \tag{1}$$

where σ is the electrical conductivity and μ_0 is the permeability. With the fluid at rest, the equilibrium magnetic stress, $B_e^2/2\mu_0$ and gravitational pressure, $\rho g x$ (ρ and g the mass density and gravitational acceleration respectively) are balanced by the pressure, p.

To linear terms in the perturbation velocity, $\mathbf{v}$, and perturbation magnetic flux density, $\mathbf{b}$, the laws of Faraday, Ampere and Ohm and flux continuity require that

$$\frac{\partial b}{\partial t} - \frac{1}{\mu\sigma}\nabla^2\mathbf{b} = \nabla\times(\mathbf{v}\times\mathbf{B}_e), \quad \nabla\cdot\mathbf{b} = 0. \tag{2), (3}$$

These relations express the effect of the fluid motion on the magnetic field.

The reciprocal effect of the fields on the motion is represented by the Navier–Stokes equation and continuity for an incompressible homogeneous fluid, written here to linear terms as

$$\rho\frac{\partial\mathbf{v}}{\partial t} = -\nabla p' + \eta\nabla^2\mathbf{v} + \nabla\cdot\mathbf{t}^m, \quad \nabla\cdot\mathbf{v} = 0, \tag{4), (5}$$

where p' is the perturbation pressure and $\mathbf{t}^m$ is the linearized magnetic stress:

$$\mathbf{t}^m = \begin{bmatrix} -\frac{1}{\mu}B_e b_z & 0 & \frac{1}{\mu}B_e b_x \\ 0 & -\frac{1}{\mu}B_e b_z & \frac{1}{\mu}B_e b_y \\ \frac{1}{\mu}B_e b_x & \frac{1}{\mu}B_e b_y & \frac{1}{\mu}B_e b_z \end{bmatrix} \tag{6}$$

Because the equations have coefficients independent of y and z, it is possible to Fourier analyse in these directions. The time dependence of the fluid motion is further represented by a complex frequency s, to be distinguished from the imposed frequency ω:

$$\mathbf{v} = \mathscr{R}\,\hat{\mathbf{v}}(x)\exp(st - jk_y y - jk_z z). \tag{7}$$

Substitution into (2) and (3) then shows that the perturbation flux density takes the form

$$\mathbf{b} = \mathscr{R}\{\hat{\mathbf{b}}^+(x)\exp[(s+j\omega)t - jk_y y - jk_z z] + \hat{\mathbf{b}}^-(x)\exp[(s-j\omega)t - jk_y y - jk_z z]\}, \tag{8}$$

where the laws are then represented by the three expressions

$$[D^2 - k^2 - \mu\sigma(s \pm j\omega)]\,\hat{b}_x^{\pm} = \tfrac{1}{2}jk_z\mu\sigma\,\hat{B}_e^{*(\mp)}(x)\hat{v}_x, \tag{9}$$

$$[D^2 - k^2 - \mu\sigma(s \pm j\omega)]\,\hat{b}_y^{\pm} = \tfrac{1}{2}jk_z\mu\sigma\,\hat{B}_e^{*(\mp)}(x)\,\hat{v}_y, \tag{10}$$

$$D\hat{b}_x^{\pm} - jk_y\hat{b}_y^{+} - jk_z\hat{b}_z^{\pm} = 0, \tag{11}$$

where $D \equiv d(\ )/dx$ and $k^2 = k_y^2 + k_z^2$. The third component of (2) is redundant. Note that these last three expressions are each two statements, one with the upper signs and operations respectively and the other with the lower signs. (Complex conjugation is represented by an asterisk.) These expressions represent the effect of the motion on the field without assumption as to the relative values of s and ω.

To represent the reciprocal effect, the flux densities of (8) are substituted into a typical term in (6) to obtain,

$$t_{xz} = \frac{1}{2\mu}\mathscr{R}[\hat{B}_e^*\hat{b}_x^+ + \hat{B}_e\hat{b}_x^-]\exp(st - jk_y y - jk_z z) + \frac{1}{2\mu}\mathscr{R}[\hat{B}_e\hat{b}_x^+ e^{2j\omega t} + \hat{B}_e^*\hat{b}_x^- e^{-2j\omega t}]\exp(st - jk_y y - jk_z z). \tag{12}$$

Thus, the stress has a time average component with the complex frequency s and a high frequency component which has no time average. Because $|s| \ll \omega$, the latter is now ignored on the grounds that inertia and viscous damping 'iron out' the high frequency response. Moreover, the complex amplitude of an entry $B_e b_i$ in (6) is $\frac{1}{2}(\hat{B}_i^*\hat{b}_i^+ + \hat{B}_e\hat{b}_i^-)$. Inclusion of additional higher frequency terms is possible, but is not done here.

Two types of internal modes can be distinguished. The first, termed longitudinal, has no vertical velocity, $\hat{v}_x$. These can be shown to be stable under a variety of boundary conditions (McHale 1977), and are not considered further here. The second type of modes are termed depth modes and are now considered in detail.

Internal depth modes

The appropriate laws are now (9)–(11) representing the effect of motion on field and (4) and (5). The latter are written with the magnetic stress time-averaged, so that all of these mechanical laws can be satisfied by the space–time dependence introduced with (7). With the mechanical equations also written in terms of the complex amplitudes, these expressions are combined to obtain two coupled equations governing the velocity and magnetic field in the fluid bulk. In writing the second of these expressions, the property $D^2\hat{B}_e = j\omega\mu\sigma\hat{B}_e$ is used.

$$(\tilde{D}^2-\tilde{\gamma}_\pm^2)\hat{\tilde{b}}_x^\pm = \frac{j\tilde{k}_z}{2}f^{(1)}(x)\hat{\tilde{v}}_x, \tag{13}$$

$$\frac{\tilde{s}}{P_m}(\tilde{D}^2-\tilde{k}^2)\hat{\tilde{v}}_x = (\tilde{D}^2-\tilde{k}^2)^2\hat{\tilde{v}}_x+\tilde{k}_z^2 M|f(x)|^2\hat{\tilde{v}}_x-2j\tilde{k}_z M[f^*(P_m\tilde{s}+2j)\hat{\tilde{b}}_x^+ +f(P_m\tilde{s}-2j)\hat{\tilde{b}}_x^-], \tag{14}$$

where variables are normalized such that

$$\tilde{D} = \delta D, \quad \tilde{k} = \delta k, \quad \tilde{s} = s/\omega P_m \quad \text{and} \quad f(x) = \hat{B}_e(x)/\hat{B}_0$$

Also,

$$\hat{\tilde{b}}^\pm = \hat{b}_x^\pm/B_0^{(1)}, \quad \hat{\tilde{v}}_x = \hat{v}_x(\mu\sigma\delta), \quad \tilde{\gamma}_\pm^2 \equiv \tilde{k}^2+2(\tilde{s}P_m \pm j). \tag{15}$$

Thus, the fundamental dimensionless parameters are

$$M = \frac{|\hat{B}_0|^2}{\mu\eta\omega}, \quad P_m = \frac{\mu\sigma\eta}{2\rho}. \tag{16}$$

With the competition of magnetic and viscous stresses represented by the magnetoviscous time $\mu\eta/B_0^2$, M will be recognized as the ratio of the time ω^{-1} characterizing the imposed field to this magnetoviscous time. If M is large, the magnetic stress can compete with the viscous stress on the time scale of the alternating applied field. Because P_m is the ratio of the magnetic diffusion time $\mu\sigma l^2$ to the viscous diffusion time $\rho l^2/\eta$, it might be termed the magnetic Prandtl number.

For purposes of studying internally coupled modes, two mechanical conditions at the upper surfaces are required. For internal modes, $\hat{v}_x = 0$ (normal velocity at an interface leads to surface coupling, the subject of the next section), and for the second either $D\hat{v}_x = 0$ (no slip condition) or $D^2\hat{v}_x = 0$ ('slippery wall', essentially the case of a free surface in the limit of an infinite gravitational force). Two electrical boundary conditions are required to determine $\hat{\mathbf{b}}$ completely. It is convenient to express these as a condition on $\hat{b}_x$ (and its derivatives), and a second condition on $\hat{b}_y$ (or $\hat{b}_z$). Since the mechanical equation, (14), involves only the x-directed field and since the mechanical boundary conditions do not involve the magnetic field at all, only the first of these is relevant to determining stability. Three simple possibilities are considered. For a perfectly conducting wall just above, it follows from Faraday's law that $\hat{b}_x^+ = \hat{b}_x^- = 0$. For an infinitely permeable wall just above, Ampere's law requires that $D\hat{b}_x^+ = D\hat{b}_x^- = 0$. With the region above free space, it follows from matching the magnetic field to a Laplacian field in the upper half-space that $D\hat{b}_x^+ + k\hat{b}_x^+ = D\hat{b}_x^- + k\hat{b}_x^- = 0$.

For these boundary conditions, it can be shown (McHale 1977) that the principle of exchange of stabilities holds. The fact that terms involving $\hat{\tilde{b}}_{\tilde{z}}^\pm$ do not couple back into the fluid equation causes the suspicion that the most critical situation is that in

which k is z-directed. This is in fact the case, as can be shown by elimination of $\hat{b}_x^{\pm}$ between (13) and (14). All terms involving M are multiplied by $\tilde{k}_z^2$.

The numerical problem is to find the values of s, M, and $\tilde{k}$ which allow non-trivial solutions of (13) and (14), and the boundary conditions. The parameters M and $\tilde{k}$ must be real and both can be considered positive. Interest is focused on: (a) the minimum value of M which gives instability for each value of $\tilde{k}$; (b) the value of $\tilde{k}$, called $\tilde{k}^*$, which gives the smallest critical value of M; and (c) the growth rates associated with $M > M^*$.

The technique used here is the common one (Betchov & Criminale 1967) of finding four linearly independent solutions to (13) and (14) which satisfy the boundary conditions at the lower surface, and testing whether it is possible for a non-trivial linear combination of these solutions to satisfy the conditions at the upper boundary. The secant method is then used to converge on the appropriate isolated, real roots.

The method used to generate the four independent solutions is different in two cases considered. In the first, and more important, case, the fluid is a lower half space bounded above by a half space of vacuum. For an infinite lower half space, the equilibrium magnetic field takes the form of (1). Then (13) and (14) become:

$$(\tilde{D}^2-\tilde{\gamma}_{\pm}^2)\,\hat{\tilde{b}}_x^{\pm} = \frac{j\tilde{k}_z}{2}\exp[(1\pm j)\tilde{x}]\,\hat{v}_x, \tag{17}$$

$$\tilde{s}(\tilde{D}^2-\tilde{k}^2)\,\hat{\tilde{v}}_x = (\tilde{D}^2-\tilde{k}^2)^2\,\hat{\tilde{v}}_x + \tilde{k}^2 M\exp[2\tilde{x}]\,\hat{\tilde{v}}_x + 4\tilde{k}_z M\,(\exp[(1-j)\tilde{x}]\,\hat{\tilde{b}}_x^{+} - \exp[(1+j)\tilde{x}]\,\hat{\tilde{b}}_x^{-}). \tag{18}$$

Terms of order $P_m s$ have been ignored. The four solutions can be formulated as infinite series of terms exponential in $\tilde{x}$ and in ascending powers of M. Explicitly, they are:

$$\hat{\tilde{v}}_x = A_n\sum_{l=0}^{\infty} D_l e^{\tilde{P}_n\tilde{x}}e^{2l\tilde{x}}; \tag{19}$$

$$\hat{\tilde{b}}_x^{\pm} = A_n\sum_{l=0}^{\infty} C_l^{\pm}\exp(\tilde{P}_n+1\pm j)\tilde{x}\exp[2l\tilde{x}]; \tag{20}$$

$$C_l^{\pm} = \frac{j\tilde{k}_z}{2[(\tilde{P}_n+1\pm j)^2-\tilde{\gamma}_{\pm}^2)]}\,D_l; \tag{21}$$

$$D_{l+1} = \frac{\tilde{k}_z^2 M D_l + 4M(C_l^{+}-C_l^{-})}{\tilde{s}[(\tilde{P}_n+2l)^2-\tilde{k}^2]-[(\tilde{P}_n+2l)^2-\tilde{k}^2]^2}. \tag{22}$$

The four solutions are specified by:

$$\text{Solution (1)},\quad D_0 = 1,\ \tilde{P}_1 = \tilde{k}; \tag{23a}$$

$$\text{Solution (2)},\quad D_0 = 1,\ \tilde{P}_2 = (\tilde{k}^2+\tilde{s})^{\frac{1}{2}}; \tag{23b}$$

$$\text{Solution (3)},\quad D_0 = C_0^{-} = 0,\ C_0^{+} = 1,\ \tilde{P}_3 = \tilde{\gamma}_{+}-(1+j); \tag{23c}$$

$$\text{Solution (4)},\quad D_0 = C_0^{+} = 0,\ C_0^{-} = 1,\ \tilde{P}_4 = \tilde{\gamma}_{-}-(1-j). \tag{23d}$$

Thus, $\hat{\tilde{v}}_x$ and $\hat{\tilde{b}}_x^{\pm}$ and their derivatives at $x = 0$ are expressed as power series in M. These series are strongly convergent, as can be seen from the recurrence relations, (21) and (22).

The four independent solutions so calculated are only independent for $\tilde{s}$ not equal to zero. For this reason, it is necessary to consider small values of $\tilde{s}$, find the

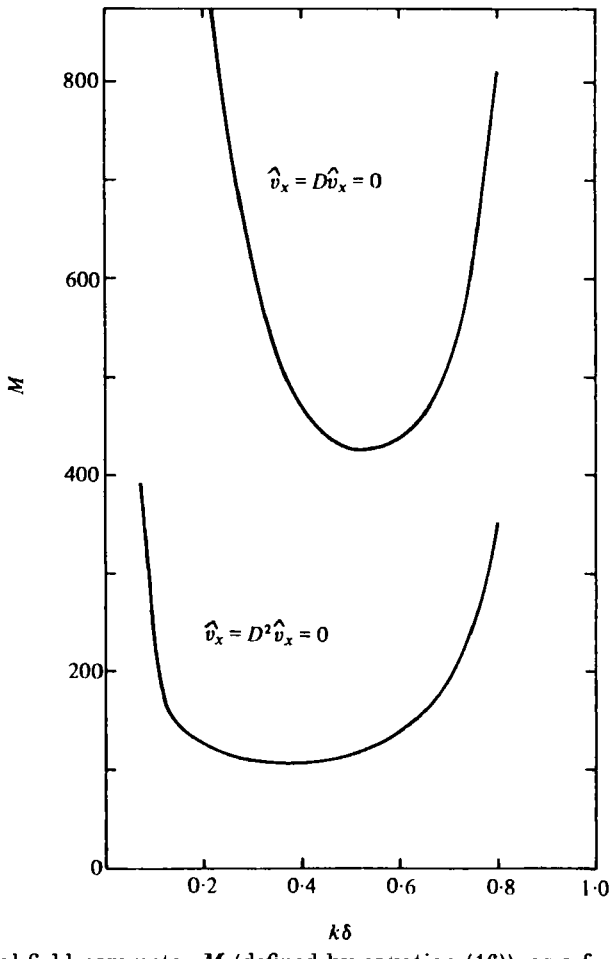

FIGURE 4. Critical field parameter M (defined by equation (16)), as a function of wavenumber normalized to the skin depth for a flat, stress-free surface (lower curve) and for a rigid flat upper boundary (upper curve).

corresponding values of M, and interpolate to find the critical value of M. In figure 4 the results of this calculation are shown for the case of the flat, stress free surface and for a flat, rigid surface. What is shown is the minimum value of M for each value of $\tilde{k}$. There are in fact other, higher values of M that are also solutions. These correspond to solutions in which $\hat{\hat{v}}_x$ and $\hat{\hat{b}}_x^+$ vary more quickly in $\tilde{x}$. In both cases there is a definite value of $\tilde{k}$ at which a minimum value of M is required for instability to occur. In the stress free case this minimum value of M is approximately 106, and occurs at $\tilde{k}$ approximately 0·4.

Other boundary conditions at $x = 0$ can be considered and result in somewhat different critical values of M, but not in a qualitatively different shape of the M *vs.* $\tilde{k}$. curve.

With the thickness of the layer finite, the form of the equilibrium magnetic field is no longer a simple exponential. This precludes the use of the above power series solutions. A predictor–corrector method is therefore used to generate the four solutions analogous to (19) and (20).

The results shown in figure 6 are for several layer thicknesses, bounded by rigid walls. Growth rates are of the same order as for the half space of liquid.

Surface effects

The boundary conditions applicable when the surface deforms are considerably more complicated than when the surface is flat.

The upper surface of the layer is assumed to be bounded by free space. The perturbation magnetic fields above the interface are then given by the gradient of a scalar potential which satisfies Laplace's equation. Since the magnetic field is sinusoidal in y and z, with wavenumbers k_y and k_z, it follows that

$$\frac{\partial b_x}{\partial x} = -kb_x. \tag{24}$$

Since there are no surface currents or magnetic materials, the following must be true:

$$\mathbf{n}.[\![\bar{B}]\!]_{x=\xi} = 0 \tag{25}$$

$$\mathbf{n}\times[\![\bar{B}]\!]_{x=\xi} = 0. \tag{26}$$

The brackets [[ ]] indicate the difference in the enclosed quantity between the upper and lower regions, and ξ is the x co-ordinate of the interface. The unit vector normal to the surface is $\bar{\mathbf{n}}$, and is given to linear terms by

$$\bar{\mathbf{n}} = \bar{\mathbf{i}}_x - \frac{\partial \xi}{\partial y}\bar{\mathbf{i}}_y - \frac{\partial \xi}{\partial z}\bar{\mathbf{i}}_z. \tag{27}$$

In terms of the Fourier-analysed variables, the boundary condition at $x = 0$ is found by combining (24), (25), (26) and (27) to linear terms:

$$D\hat{b}_x^{\pm} + k\hat{b}_x^{\pm} = -jk_z\frac{\hat{v}_x}{s}\frac{d\hat{B}_z}{dx}. \tag{28}$$

Use is made here of the fact that, to linear terms,

$$s\hat{\xi} = \hat{v}_x(x=0). \tag{29}$$

The mechanical boundary conditions result from consideration of force balance for the interface:

$$[\![S_{ij}]\!]n_j + [\![T_{ij}]\!]n_j + n_i\gamma\left(\frac{\partial^2\xi}{\partial y^2} + \frac{\partial^2\xi}{\partial z^2}\right) = 0. \tag{30}$$

The surface tension is γ, and S_{ij}, the viscous stress tensor, is given by

$$S_{ij} = -p\delta_{ij} + \eta\left(\frac{\partial v_i}{\partial x_j} + \frac{\partial v_j}{\partial x_i}\right). \tag{31}$$

Using equations (7), (19), (24) and (31), the x component of (30) can be written as

$$\begin{aligned} 0 = {} & \left(k^2\gamma + \rho g + \frac{k_z^2}{k^2}\frac{|\hat{B}_0|^2}{2\mu\delta}\right)\hat{v}_x + 3\eta s D\hat{v}_x + \frac{\rho s^2}{k^2}D\hat{v}_x \\ & - \frac{\eta}{k^2}sD^3\hat{v}_x + \frac{s}{2\mu k^2}\left\{\hat{B}_0^*\, jk(k-k_z)\,\hat{b}_x^+ + \hat{B}_0\, jk(k-k_z)\,\hat{b}_x^- \right. \\ & \left. - \frac{\hat{B}_0^*(1-j)jk_z}{\delta}\hat{b}_x^+ - \frac{\hat{B}_0(1+j)jk_z}{\delta}\hat{b}_x^-\right\}. \end{aligned} \tag{32}$$

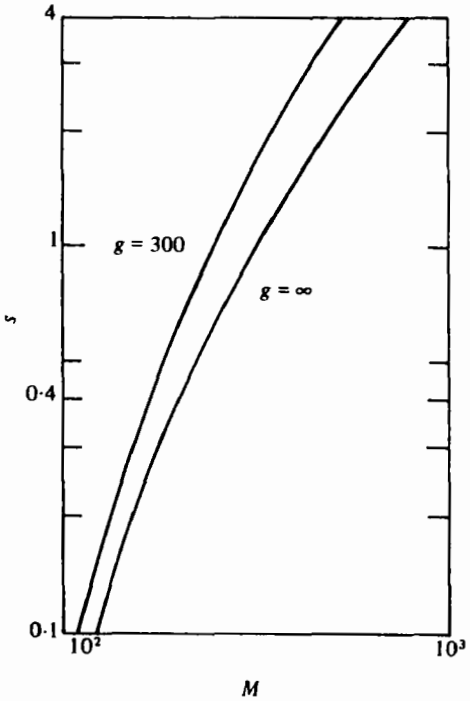

FIGURE 5. Growth rate *vs.* field parameter M for free and rigid surfaces. Normalizations of s and the 'gravitational' parameter g are given with (14) and (36). $k\delta = 0{\cdot}4$.

The other boundary condition on $\hat{v}_x$ results from consideration of the y and z components of (30), which to linear terms are

$$\eta\left(\frac{\partial v_y}{\partial x}+\frac{\partial v_x}{\partial y}\right)=0, \quad \eta\left(\frac{\partial v_z}{\partial x}+\frac{\partial v_x}{\partial z}\right)=0. \tag{33), (34}$$

Using continuity and transforming to the complex variables:

$$D^2\hat{v}_x+k^2\hat{v}_x=0. \tag{35}$$

The boundary conditions are thus condensed into four conditions on $\hat{b}_x^{\pm}$, $\hat{v}_x$ and their derivatives. Again, to determine fully the y and z components of the magnetic field requires another set of boundary conditions in the same manner as in the previous case. But, as there, these do not affect the problem of stability because the y and z directed field coupling with the fluid is expressed in (32) and (14) in terms of $\hat{b}_x$ and its derivatives. This involves combining the actual physical boundary conditions and effectively ignores three boundary conditions involving $\hat{b}_y^{\pm}$ and $\hat{v}_y$. The question is left open as to whether these conditions are satisfied by solutions of the condensed set of boundary conditions, if k_y is finite.

This dilemma of satisfying an extra three boundary conditions is met by considering the fact that there is an additional set of modes independent from those described by (20) and (21). These additional modes are those for which $\hat{v}_x$ is identically zero. It can be shown (McHale 1977) that the additional modes that result by considering these extra solutions are all stable, and that unstable solutions resulting from considering only (35), (38) and (42) are unaffected by the extra solutions.

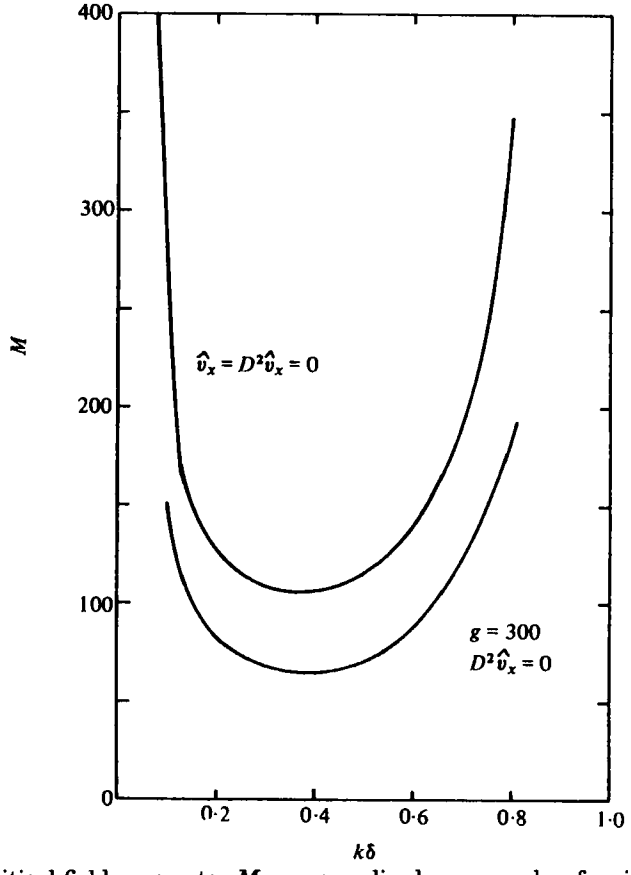

FIGURE 6. Critical field parameter M *vs.* normalized wavenumber for rigid and free boundaries with the parameter g normalized as in (36).

For the natural frequencies associated with essentially gravity-capillary surface waves, for all values of k, the effect of the field is to increase the imaginary part of s and to increase the rate of decay. In no case is the field destabilizing.

The waves that are essentially internally coupled modes have somewhat lower M in the case of a free surface than if the surface is flat. By means of figure 5, the growth rates and critical field parameters associated with the case of a flat surface, (gravity infinite) and the case in which gravity has a value typifying actual experimental conditions are compared.

When the normalization is introduced into (32) the natural dimensionless gravity constant is

$$\tilde{g} = \frac{\rho g \delta}{\eta \omega}. \tag{36}$$

For actual experimental conditions $\tilde{g}$ is approximately 300. The inclusion of the free surface is moderately destabilizing, as shown in figure 6.

T_m, melting point	47 °C
ρ, mass density	$8{\cdot}8 \times 10^3$ kg m^{-3}
c_p, specific heat	150 J K^{-1} kg^{-1}
H_f, heat of fusion	$1{\cdot}4 \times 10^4$ J kg^{-1}
k, thermal conductivity	16·5 W m^{-1}
σ, electrical conductivity	2×10^6 mho m^{-1}
η, absolute viscosity	$\sim 5 \times 10^{-4}$ kg m^{-1} s^{-1}

TABLE 1. Properties of Cerelow-117 alloy
(Bi 44·7%, Pb 22·6%, In 19·1%, Sn 8·3%, Cd 5·3%).

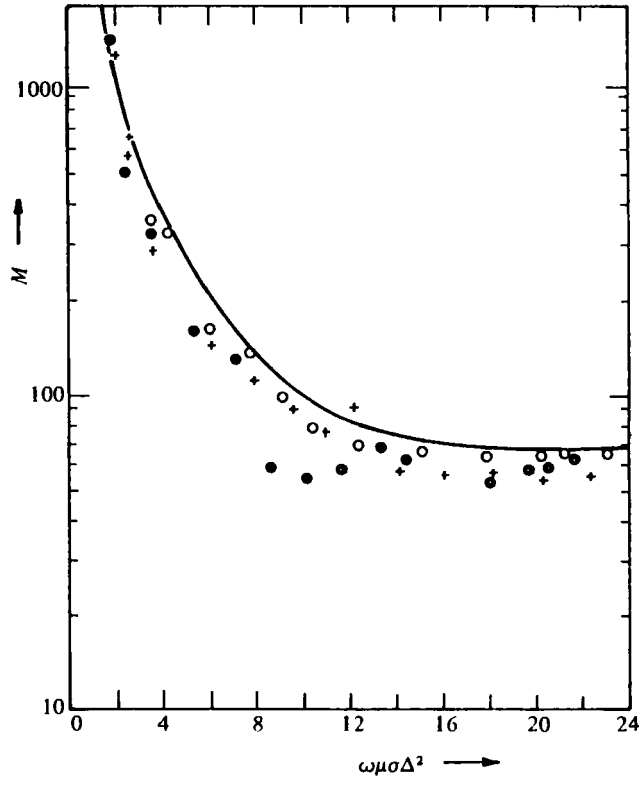

FIGURE 7. Observed critical field parameter M *vs.* normalized frequency. ○, glass dish, $\Delta = 1{\cdot}5$ cm; ●, glass dish, $\Delta = 2{\cdot}2$ cm; +, copper dish, $\Delta = 1{\cdot}5$ cm.

3. Experimental results

The experimental apparatus is shown in figure 1. Three separate coils are driven so as to make the field above the fluid surface as uniform as possible. Measurements indicate a maximum field inhomogeneity of 5%.

The liquid metal used is a low melting point commercial alloy of lead, tin, and bismuth (Cerrelow-117). The properties of the alloy are shown in table 1. The surface of the metal is covered with a thin layer of weak hydrochloric acid to retard the formation of surface film. An isolation cell is suspended in the centre of a larger container to reduce end and edge effects.

Further details of the experimental apparatus are given in McHale (1977).

The critical field strength is observed as the frequency is continuously varied. Different depths of fluid are used. In figure 7 the experimental data is summarized in non-dimensional form. The solid curve in that figure is constructed from the theory of the previous section. At low values of $\omega\mu\sigma\Delta^2$ the critical value of M is a strong function of that argument, while for large values, M^* asymptotically approaches the value given by the theory for an infinite lower half space. Experimental values are consistently slightly lower than those theoretically predicted but within errors introduced by uncertainties in property values.

4. Discussion and conclusions

Measurements of critical field strength required for instability are in good agreement with the prediction based on the linear hydromagnetic stability theory. It seems clear that the undulations have an origin relating to the electromechanical mode. However, a further observation makes it clear that the primary source of energy for what is observed does not come from the purely electromechanical processes that have been described.

When the field is turned on suddenly, the observed time for the motion to increase from essentially nothing to its final saturation value is one to ten seconds. Whether or not the free surface effects are included, none of the growth rates predicted by the electromechanical model developed here is this short. Typically, the instability is predicted to grow at rates of 100 to 1000 seconds.

Motivated by this discrepancy, a lumped parameter model that includes thermal effects has been developed (McHale & Melcher 1978). This model suggests that what is observed is driven by eddy current heating, but takes on its character from the electromechanics. In effect, the processes described here result in certain circulations being accelerated by a negative damping. The combination of eddy currents, both in the liquid and in the container as determined by contact resistance, and cooling from the upper surface, can result in net heating of the fluid from below or from the side. For both cases, the resulting motion should appear, by the lumped parameter model, in 5–8 seconds, consistent with experimental results.

Some experiments demonstrate the augmentation of heat transfer caused by the electromechanics (McHale & Melcher 1978). However, future work in this area should recognize that the undulations can be driven by the heating, with the electromechanics effectively decreasing the damping. This should also occur in shear flows, where the drive can come from an equilibrium fluid velocity. Shear flows are more attractive theoretically because purely thermal instability can occur for very small heating.

For a given frequency and fluid, the critical value of M determines the maximum depth of fluid that can be levitated or depressed magnetically without causing surface undulations or augmentation of heat and mass transfer. This is true because both M and the magnetic pressure depend on B_0^2. (Melcher 1981). For example, a layer having thickness L would be levitated if $\rho Lg = B_0^2/4\mu$, and so the greatest thickness that could be levitated without the electromechanical instability would be $L = \eta\omega M^*/4\rho g$.

This work was performed as a part of the program 'Machine Casting of Ferrous Alloys' carried out at MIT under the leadership of Professor Merton C. Flemings and sponsored by DARPA.

REFERENCES

BETCHOV, R. & CRIMINALE, O. 1967 *Stability of Parallel Flows*, chap. 3. Academic.

CHANDRASEKHAR, S. 1961 *Hydrodynamic and Hydromagnetic Stability*. Clarendon.

FRASER, M. E., LU, W. K., HAMICLEC, A. E. & MURARKA, R. 1971 Surface tension measurements on pure liquid iron and nickle by an oscillating drop technique. *Metallurgical Trans.* **2**, 817.

HOFFMAN, K. & KUNZE, R. 1961 *Linear Algebra*. Prentice-Hall.

MCHALE, E. J. 1977 AC magnetohhydrodynamic instability, Ph.D. thesis, Department of Electrical Engineering, Massachusetts Institute of Technology.

MCHALE, E. J. & MELCHER, J. R. 1978 Hydromagnetic instability of liquid metals in AC magnetic fields, and augmentation of heat transfer. *Electric Machines & Electromech.* **3**, 197.

MELCHER, J. R. 1981 *Continuum Electromechanics*, pp. 6.20–6.22 and 8.1–8.15. MIT Press.

MELCHER, J. R. & HURWITZ, M. 1970 U.S. Patent 3,496,736.

SCHAFFER, M. 1966 *Hydromagnetic Surface Waves with an Alternating Magnetic Field*. Ph.D. thesis, Department of Electrical Engineering, Massachusetts Institute of Technology.

SCHAFFER, M. 1968 Hydromagnetic surface waves with alternating magnetic fields. *J. Fluid Mech.* **4**, 337.

SUNDERLAM, T. 1973 Thermal diffusion in kinetic and equilibrium measurements by a levitation technique. *Metallurgical Trans.* **4**, 575.